# INVESTIGATE THE EFFECT OF ORTHOPEDIC METAL ARTEFACT REDUCTION ALGORITHM ON DOSIMETRY OF IMRT PROSTATE WITH HIP PROSTHESIS

### NURUL NAJAH BINTI MOHD ZAKIR

### SCHOOL OF HEALTH SCIENCE UNIVERSITI SAINS MALAYSIA

# INVESTIGATE THE EFFECT OF ORTOPEDIC METAL ARTEFACT REDUCTION ALGORITHM ON DOSIMETRY OF IMRT PROSTATE WITH HIP PROSTHESIS

by

### NURUL NAJAH BINTI MOHD ZAKIR

Dissertation submitted in partial fulfilment of the requirements for the degree of Bachelor of Medical Radiation (Honours)

### **CERTIFICATE**

This is to certify that the dissertation entitled Investigate the Effect of Ortopedic Metal Artefact Reduction Algorithm on Dosimetry of IMRT Prostate with Hip Prosthesis is the bona fide record of research work done by Ms. Nurul Najah binti Mohd Zakir during the period from October 2024 to July 2025 under my supervision. I have read this dissertation and that in my opinion it conforms to acceptable standards of scholarly presentation and is fully adequate, in scope and quality, as a dissertation to be submitted in partial fulfilment for the degree of Bachelor of Medical Radiation (Honours).

Main supervisor,	Field supervisor,
Dr. Jayapramila A/P Jayamani	Ms. Arifah Nazirah binti Abdullah
Lecturer	Medical Officer
School of Health Science	School of Health Science
Universiti Sains Malaysia	Universiti Sains Malaysia
Health Campus	Health Campus
16150 Kubang Kerian	16150 Kubang Kerian
Kelantan, Malaysia	Kelantan, Malaysia
Date:	Date:
2	2

**DECLARATION** 

I hereby declare that this dissertation is the result of my own investigations, except

where otherwise stated and duly acknowledged. I also declare that it has not been

previously or concurrently submitted as a whole for any other degrees at Universiti

Sains Malaysia or other institutions. I grant Universiti Sains Malaysia the right to use

the dissertation for teaching, research, and promotional purposes.

.....

Nurul Najah binti Mohd Zakir

Date: .....

iii

### **ACKNOWLEDGMENT**

All praise and gratitude to Allah SWT, for granting me the strength, patience, and guidance to complete this thesis. Without his blessings, this accomplishment would not have been possible.

I want to extend my deepest appreciation to my parents, Mr. Mohd Zakir Abu Bakar and Mrs. Roslin Abdul Razak, whose unwavering love, prayers, and continuous encouragement throughout this academic journey. To my two sisters, Nurul Najwa and Nur Diyana, thank you for always cheering me on and sharing both laughter and tears. To my brothers, Faiq Wazif and Fahim Waiz, thank you for always believing in me as a sister.

I am sincerely thankful to my main supervisor and field supervisor, Dr. Jayapramila A/P Jayamani, and Ms. Arifah Nazirah Abdullah, and Madam Nor Shazleen Ab. Shukor for their expert guidance, insightful feedback, and invaluable advice. A special thanks to the dedicated JPNRO staff who contributed significantly to the success of this study and assisted me during my research.

And lastly, to my big heart friends, thank you for being my pillars of strength and understanding, both in the high and low moments. Your companionship has made this academic journey less daunting and far more meaningful.

### TABLE OF CONTENTS

CERTIFICATE	ii
DECLARATION	iii
ACKNOWLEDGMENT	iv
ABSTRAK	ix
ABSTRACT	xi
LIST OF TABLES	xii
LIST OF FIGURES	xiii
LIST OF SYMBOLS	xvi
LIST OF ABBREVIATIONS	xviii
LIST OF APPENDICES	xx
CHAPTER 1	1
INTRODUCTION	1
1.1 Study Background	1
1.2 Problem Statement	3
1.3 Objectives	4
1.3.1 General Objective	4
1.3.2 Specific Objective	4
1.4 Hypothesis	4
1.4.1 Null Hypothesis	4
1.4.2 Alternative Hypothesis	4
1.5 Significance of Study	5

CHAPTER	2 LITERATURE REVIEW	6
2.1 Pr	ostate Cancer	6
2.1.1	Prostate Cancer in Malaysia	7
2.1.2	Cancer Symptoms and Diagnosis	8
2.1.3	Treatment for Prostate Cancer	10
2.2 Ra	adiation Therapy	10
2.2.1	External Beam Radiation Therapy	11
2.2.2	Linear Accelerator	12
2.2.3	IMRT Treatment Technique	13
2.3 Hi	p Prosthesis in Radiotherapy	14
2.3.1	Metal Artifact Reduction Technique	15
2.3.2	OMAR Algorithm in Radiotherapy	16
2.4 Th	nermoluminescence Dosimeter	18
2.4.1	TLD Principle	19
CHAPTER	3 MATERIALS AND METHODOLOGY	21
3.1 M	aterials	21
3.1.1	TLD-100	21
3.1.2	TLD Programmable Annealing Oven	22
3.1.3	TLD Slack and Annealing Tray	23
3.1.4	TLD Reader System	24
3.1.5	Solid Water Phantom and Bolus	25
3.1.6	Varian Clinax iX LINAC	26

3.1.7	In-house Pelvic Phantom and Hip Prosthesis	27
3.1.8	CT Simulator	29
3.1.9	Eclipse TPS	30
3.1.10	ImageJ Software	31
3.2 N	Methodology	31
3.2.1	TLD-100 Calibration	32
3.2.2	TLD Reading	33
3.2.3	CT Simulation	36
3.2.4	IMRT Technique Planning	39
3.2.5	Irradiation of In-House Pelvic Water Phantom	40
3.3 S	tudy Flowchart	42
CHAPTEI	R 4 RESULTS AND DISCUSSION	43
4.1 Т	LD-100 Calibration	43
4.2 V	Validation of In-House Pelvic Phantom	45
4.3	CT Image Evaluation on Metal Artefact	48
4.4 Г	Oose Verification Using In-house Pelvic Phantom	50
4.4.1	IMRT Treatment Evaluation	50
4.4.2	Point Dose Evaluation in TPS Calculation	53
4.5 S	ummary of CT Number and Point Dose Analysis	59
4.6 I	imitation of Study	59
CHAPTEI	R 5	61
	SION	61

APPEN	DICES	69
REFER	RENCES	63
5.2	Future Recommendations	62
5.1	Conclusion	61

### MENYIASAT KESAN ALGORITMA "ORTHOPEDIC METAL ARTIFACT REDUCTION" TERHADAP DOSIMETRI IMRT PROSTAT DENGAN PROSTESIS PINGGUL

### **ABSTRAK**

Kanser prostat merupakan salah satu kanser yang paling kerap berlaku dalam kalangan lelaki di Malaysia, dan radioterapi—khususnya Terapi Sinaran Termodulasi Keamatan (IMRT)—merupakan rawatan utama. Namun, kehadiran implan pinggul logam dalam sesetengah pesakit boleh menyebabkan artifak dalam imej tomografi berkomputer (CT), yang menjejaskan ketepatan anatomi dan pengiraan dos radiasi. Kajian ini menyiasat kecekapan algoritma "Orthopedic Metal Artifact Reduction" (OMAR) oleh Philips dalam mengurangkan artifak tersebut dan meningkatkan ketepatan dos dalam IMRT untuk kanser prostat. Sebuah fantom pelvis lelaki khas dengan implan pinggul logam dibina menggunakan bahan setara tisu dan disinarkan dengan pancaran foton 6 MV. Dos radiasi dikira menggunakan Sistem Perancangan Rawatan (TPS) Eclipse dan disemak menggunakan dosimeter TLD-100 yang telah dikalibrasi. Keputusan menunjukkan bahawa algoritma **OMAR** berjaya mengurangkan herotan imej dengan ketara dan meningkatkan ketepatan pelakuran struktur serta penyampaian dos. Pelan rawatan berdasarkan imej yang diperbetulkan dengan OMAR menunjukkan kesesuaian dan kehomogenan dos yang lebih baik. Ujian statistik mengesahkan peningkatan ketara dalam ketepatan dos (p < 0.05) pada beberapa organ. Kajian ini membuktikan bahawa penggunaan algoritma OMAR meningkatkan kualiti imej dan ketepatan dos radiasi, menjadikannya alat yang bernilai dalam perancangan rawatan radioterapi bagi pesakit yang mempunyai implan logam.

Kata kunci: OMAR algoritma, pengurangan artifak logam, IMRT

INVESTIGATE THE EFFECT OF ORTHOPEDIC METAL

ARTIFACT REDUCTION ALGORITHM ON DOSIMETRY OF

IMRT PROSTATE WITH HIP PROSTHESIS

**ABSTRACT** 

Prostate cancer is one of the most common cancers among Malaysian men, and

radiotherapy—especially intensity-modulated radiation therapy (IMRT)—is a key

treatment. However, metal hip implants in some patients can cause artefacts in

computed tomography (CT) images, which affect the accuracy of anatomy and

radiation dose calculations. This study investigated the efficiency of the Orthopedic

Metal Artifact Reduction (OMAR) algorithm by Philips reduces these artefacts and

improves dose accuracy in prostate IMRT. A custom male pelvic phantom with a metal

hip implant was created using tissue-like materials and treated with a 6 MV photon

beam. The radiation doses were calculated using the Eclipse treatment planning system

(TPS) and checked using a calibrated thermoluminescent dosimeter (TLD) type 100.

The results showed that OMAR significantly reduced image distortion and improved

the accuracy of structure outlines and dose delivery. Treatment plans based on OMAR-

corrected images had better dose conformity and uniformity. Statistical tests confirmed

significant improvements in dose accuracy (p > 0.05) in several organs. Hence, the

OMAR algorithm has been proven that it improve both image quality and radiation

dose accuracy, making it a valuable tool for radiotherapy planning in patients with

metal implants.

Keywords: OMAR algorithm, metal artefact reduction, IMRT

хi

### LIST OF TABLES

Table 3.1The density of human and the material selected for the male pelvic phant	om
construction. Measured value using Archimedes' principle compared w	vith
the NIST X-COM value (Jayamani et al., 2023)	29
Table 3.2 The guidelines of dose constraint of the IMRT prostate plan (Abu-Gheid	a et
al., 2019)	39
Table 4.1 Physical density and CT number analysis of the in-house pelvic phant	om
materials compared with the actual human tissues	45
Table 4.2 The dosimetric outcomes of the IMRT prostate on PTV and OARs in	the
Reference, W-OMAR, and OMAR CT images	51
Table 4.3 Statistical analysis of TPS calculated dose and TLD measured dose	for
IMRT prostate with metal hip prosthesis using the Paired T test	57

### LIST OF FIGURES

Figure 2.1 The anatomy of the prostate (Cleveland Clinic, 2017)Error! Bookmark
not defined.
Figure 2.2 The difference in age-specific incidence rate in Malaysia between 2012-
2016 (National Cancer Institute Malaysia, 2023) 7
Figure 2.3 The staging of prostate cancer (American Urological Association, 2018) 8
Figure 2.4 The DRE test for prostate cancer diagnosis (American Urological
Association, 2018)
Figure 2.5 Schematic diagram of LINAC (Morrow et al., 2019)
Figure 2.6 Dark streak (red arrow) and bright streak (yellow arrow) caused by a metal
artefact in the CT image (Puvanasunthararajah et al., 2021)
Figure 2.7 The principle of Philips' OMAR algorithm in mitigating the metal-induced
artefacts in CT images (Puvanasunthararajah et al., 2021)
Figure 2.8 Various forms of the TLD that are commercially used
Figure 2.9 The principle of TLD
<b>Figure 3.1</b> A TLD-100 chip 22
Figure 3.2 The TLD programmable annealing oven at the Medical Radiation
Laboratory, PPSK 23
Figure 3.3 TLD slack and TLD annealing tray 24
Figure 3.4 The TLD reader system installed at the Medical Radiation Laboratory,
PPSK 25
Figure 3.5 The solid water phantom with various thicknesses and a 1.0 cm thick bolus
26
Figure 3.6 The Varian Clinax iX LINAC installed at JPNRO, HPUSM 27

Figure 3.7 The (a) in-house pelvic phantom with (b) bladder, (c) prostate, (d) rectum,
(e) femoral head, and (f) metal fiber hip prosthesis 28
Figure 3.8 The CT simulator installed at the JPNRO, HPUSM 30
Figure 3.9 An annealing tray with TLD-100 chips positioned in the annealing oven
32
<b>Figure 3.10</b> Calibration set up for TLD-100 under 6 MV photon beam 33
Figure 3.11 The Thermo Scientific WinREMS operational software 34
Figure 3.12 A TLD-100 on the stainless-steel planchet of the TLD reader machine 35
Figure 3.13 The positions of TLD-100 chips on the phantom (a) bladder, (b) prostate,
(c) rectum, (d) femoral head, and (e) metal hip prosthesis from the above
(left) and side (right) views 36
Figure 3.14 The setup of an in-house pelvic phantom without (left) and with metal
(right) for CT simulation 37
Figure 3.15 An ROI drawn on the within the OAR on the Reference CT DICOM
image 38
Figure 3.16 The line profile drawn across the ROI on the selected slice of the
Reference CT image 38
Figure 3.17 The setup of in-house pelvic phantom with metal implant for irradiation
based on IMRT prostate planned 41
Figure 3.18 The study workflow of investigate the OMAR algorithm effect in
dosimetry for IMRT prostate with hip prosthesis 42
Figure 4.1 The Si of the TLD-100
Figure 4.2 Plot profile of CT number in HU for the Reference, W-OMAR, and OMAR
CT images 48

Figure 4.3 Dose distribution of IMRT prostate in the (a) Reference, (b) W-OMAR
and (c) OMAR 51
Figure 4.4 Comparisons of point dose calculated in TPS between Reference, W-
OMAR, and OMAR at the specific point of (a) bladder, (b) prostate, (c)
rectum, and (d) left femoral head. The bar chart is presented with a 5%
error bar. 54

### LIST OF SYMBOLS

cGy Centigray

cm Centimeter

°C Degree Celcius

 $D_{x\%}$  Dose received by x% of the PTV

g/cm<sup>3</sup> Gram per cubic centimeter

Gy Gray

HU Hounsfield Unit

CF<sub>i</sub> Individual calibration factor

S<sub>i</sub> Individual sensitivity factor

Kv Kilovolt

< Less than

D<sub>max</sub> Maximum dose

MV Megavolt

μC Microcoulomb

MeV Mega electron volt

mAs Mili Amphere per second

MU Monitor Unit

> More than

nC Nanocoulomb

% Percent

ρ Physical density

± Plus-minus

### LIST OF ABBREVIATIONS

**3D CRT** Three-Dimensional Conformal Radiation Therapy

AAA Anisotropic Analytical Algorithm

**CBCT** Cone Beam Computed Tomography

CI Conformity Index

CT Computed Tomography

CTDI Computed Tomography Dose Index

**DICOM** Digital Imaging and Communications in Medicine

**DVH** Dose Volume Histogram

**EBRT** External Beam Radiation Therapy

HI Homogeneity Index

HU Hounsfield Unit

**HPUSM** Hospital Pakar Universiti Sains Malaysia

**IMRT** Intensity Modulated Radiation Therapy

LINAC Linear Accelerator

MLC Multi-leaf Collimator

NIST National Institute of Standards and Technology

OAR Organ at Risk

OMAR Orthopedic Metal Artifact Reduction

OBI On-board Imager

PPSK School of Health Science (Pusat Pengajian Sains Kesihatan)

PTV Planning Target Volume

**RED** Relative Electron Density

**ROI** Region of Interest

**SD** Standard Deviation

**TLD** Thermoluminescent Dosimeter

**TPS** Treatment Planning System

**USM** Universiti Sains Malaysia

VMAT Volumetric Modulated Arc Therapy

W-OMAR Without Orthopedic Metal Artifact Reduction

### LIST OF APPENDICES

APPENDIX A RAW DATA OF TLD CALIBRATION UNDER 6 M PHOTON
BEAM

APPENDIX B RAW DATA OF CT NUMBER ANALYSIS

APPENDIX C RAW DATA OF POINT DOSE CALCULATED IN THE IMRT REFERENCE, W-OMAR, AND OMAR CT IMAGES

APPENDIX D RAW DATA OF TLD MEASURED USING TLD-100 ON IMRT
OMAR

APPENDIX E RAW DATA OF THE STATISTICAL PAIRED T TEST

### **CHAPTER 1**

### INTRODUCTION

### 1.1 Study Background

According to the Malaysia National Cancer Registry Report (2017-2021), prostate cancer is the third most common cancer among men in Malaysia, with an incidence rate of 3.8% (National Cancer Institute Malaysia, 2023) Prostate cancer is a type of cancer that develops in the prostate, a small walnut-shaped gland located beneath the bladder and in front of the rectum in males. Some of these prostate cancer patients have a hip prosthesis implant, also known as metal implants, which are manmade metal joints that replace a damaged hip joint during a hip replacement surgery procedure. This metal implant is commonly made of titanium (density and atomic number of 4.51 g/cm<sup>3</sup> and 22, respectively). Several challenges arise from the physical and imaging properties of the metal, specifically due to its high density and atomic number, which can alter the planned radiation dose distribution and lead to significant artefacts in computed tomography (CT) images.

Radiotherapy is one of the treatments for prostate cancer that employs radiation to kill the cancer cells and shrink the tumour (Chandra *et al.*, 2021). In radiotherapy, patients will go through CT simulation to obtain the CT images used for treatment planning. The CT DICOM contrast and greyscale observed on CT scans are formed by the different amounts of radiodensity inside the bone and soft tissue structures, allowing the viewing of smaller features (Ramesh *et al.*, 2023). Furthermore, the radiodensity is numerically represented in Hounsfield Units (HU), which is the

computed value that reflects the x-ray attenuation coefficient in an image voxel, while relative electron density (RED) is the electron density of a material in relation to the electron density of water (Ramesh *et al.*, 2023).

Since metal implants have a very high radiodensity, more than 3000 HU, compared to the surrounding tissues, it will cause significant artefacts in CT images. The artefacts created in the CT image produced may increase the inaccuracy of the structure visualization, inaccurate HU, and RED values. The artefacts will mask the surrounding tissues and distort the anatomical details (Neroladaki *et al.*, 2019). Regarding these artefacts, there are various algorithms used nowadays to reduce the metal artefacts in the CT images.

The metal artefact reduction (MAR) algorithm, which is in-built into the CT to reduce the artefacts caused by the metal implants. The MAR will identify the metal object as the high-density region in the image and correct the data before reconstructing the image (King *et al.*, 2022). The resulting image will significantly reduce metal artefacts, making it easier to visualize the tissues and structures surrounding the metal implants. Different manufacturer has different MAR algorithms, such as Siemens' IMAR, Philips' OMAR, GE's MARs, and Canon's SEMAR.

In this study, a heterogeneous male pelvis phantom is modelled and evaluated with the thermoluminescent dosimeter (TLD) type TLD-100 chips together with Philips' OMAR algorithm. The absorbed dose from the IMRT prostate plan is studied to validate the accuracy of dose calculation in the treatment planning system (TPS).

### 1.2 Problem Statement

In radiotherapy, accurate dose calculation is crucial for effective treatment planning and delineation. However, the presence of metal implants in patients causes artefacts in CT DICOM images since they have much higher densities compared to human tissues. These artefacts can distort the image quality and produce incorrect HU values, impacting the accuracy of the radiation dose delivered to the tissues surrounding the implant. The artefacts will form in bright and dark streaking near the metal implant, covering the surrounding soft tissues and distorting the organ's visualization (Gnanasambandam *et al.*, 2022).

Metal artefacts create incorrect HU readings in the area surrounding the implants. Since the TPS relies on the HU values to determine the electron density for dose calculations, the misrepresentation of tissue density will lead the TPS to overestimate or underestimate the radiation dose given to the tissues near the metal. For example, dose errors of up to 8.4% at the isocenter have been reported when artefacts are uncorrected (Banaee *et al.*, 2021; Ziemann *et al.*, 2018). Then, those incorrect HU values affect the calculation of monitor units (MU), which influence the amount of radiation delivered. A study shows that a failed corrected metal artefact can increase the required MUs by several units per fraction, resulting in systematic dose delivery errors over the entire treatment course (Banaee *et al.*, 2021). Hence, it leads to inaccuracies in dose calculation, directly results in inadequate treatment outcomes, and increases the risk of complications.

This study aims to investigate the effect of Philips' OMAR techniques on the accuracy of dose calculation in radiotherapy. The primary aim of OMAR methods is to minimize these artefacts, thereby enhancing image quality, improving contouring accuracy for tumors and organs at risk. OMAR techniques have shown promise in

eliminating metal artefacts and enhancing dose distribution accuracy (Cao *et al.*, 2022). This technique works by mitigating metal artefacts in CT images, allowing for a more precise dose calculation in radiotherapy planning and ultimately leading to better treatment outcomes.

### 1.3 Objectives

### 1.3.1 General Objective

To evaluate the OMAR algorithm's efficiency on dose calculation with a metal hip prosthesis in IMRT prostate.

### 1.3.2 Specific Objective

- To analyse the CT number profile between the reference, W-OMAR, and OMAR CT images on the in-house pelvis phantom.
- 2. To plan and calculate the dose distribution for IMRT prostate in the CT images using Eclipse TPS.
- To compare the calculated and measured dose using the TLD-100 on the phantom.

### 1.4 Hypothesis

### 1.4.1 Null Hypothesis

There is no significant difference in the dose calculated between the W-OMAR and OMAR.

### 1.4.2 Alternative Hypothesis

There is a significant difference in the dose calculated between the W-OMAR and OMAR.

### 1.5 Significance of Study

By addressing the critical limitation created by the metal artefacts in radiotherapy planning, this study significantly evaluates the effectiveness of the OMAR algorithm in mitigating the imaging distortions caused by the high-density metal hip prosthesis. The presence of metal during the CT scans produces metal artefacts in the CT DICOM images, which can mask the surrounding tissues' anatomical structures and affect the accuracy of dose distribution in radiotherapy treatment. As a result, by investigating the efficacy of OMAR in improving the quality of the CT images and dose calculations, this study provides the empirical evidence to support its implementation in clinical practice. Additionally, it will directly give implications for patient safety and treatment outcomes.

### **CHAPTER 2**

### LITERATURE REVIEW

### 2.1 Prostate Cancer

Prostate cancer is a type of cancer that arises in the prostate gland, which is located at the base of the bladder and in front of the rectum. The main function of the prostate in the male reproductive system is to produce fluid, which is a component of semen (Toivanen and Shen, 2017). Even though many prostate cancer cases grow slowly and remain confined in the gland, there are some that can grow and spread quickly to other parts of the body, for example, bones and lymph nodes. The mutation occurring in the DNA leads the cells in the prostate glands to grow uncontrollably, multiplying faster and living longer than normal cells, eventually developing tumours that can damage surrounding tissues (Cleveland Clinic, 2023).

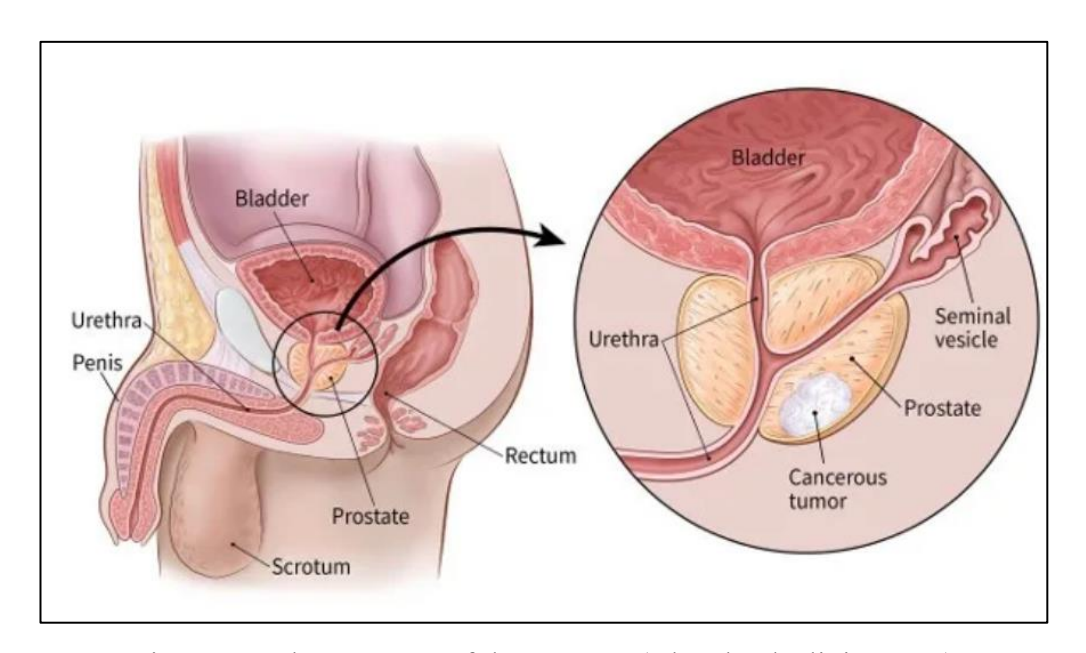


Figure 2.1 The anatomy of the prostate (Cleveland Clinic, 2017)

### 2.1.1 Prostate Cancer in Malaysia

Prostate cancer is a significant public health issue throughout Malaysia, ranking third among male malignancies, with a lifetime risk estimated between 1 in 94 and 1 in 117 men (Lim *et al.*, 2021). Additionally, statistic from the Malaysia National Cancer Registry Report (2017-2021) shows that about 67.0% of prostate cancer patients in Malaysia were diagnosed in the last stage (National Cancer Institute Malaysia, 2023). This leads to significantly lower survival chances, emphasising the crucial need for early identification. The figure demonstrates that it primarily affects males aged 50 and older, with the largest prevalence occurring in individuals aged 75 years and above (National Cancer Institute Malaysia, 2023). The Malaysia Prostate Cancer (M-CaP) Study observed that ethnic distribution reveals greater frequency among Malay men, followed by Indian and Chinese men, with some research indicating Chinese men as the most diagnosed, reflecting Malaysia's multi-ethnic population (Lim *et al.*, 2021).

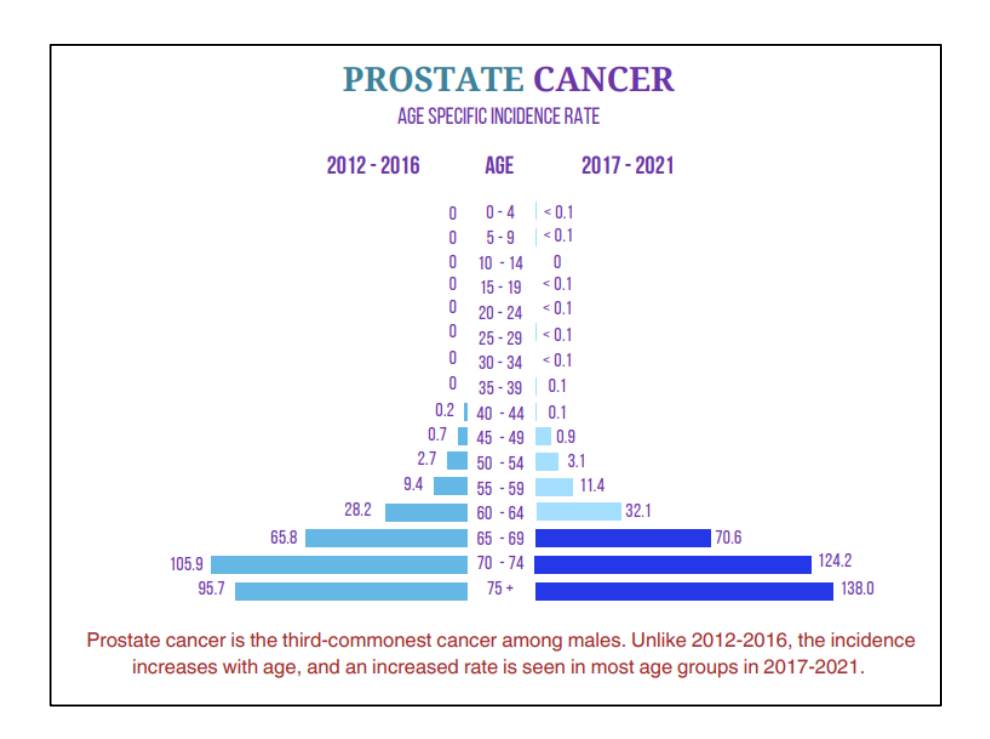


Figure 2.2 The difference in age-specific incidence rate in Malaysia between 2012-2016 (National Cancer Institute Malaysia, 2023)

### 2.1.2 Cancer Symptoms and Diagnosis

The characteristics of the tumour cells determine the stage of the cancer, which is based on its size and the progression to spread to other parts of the body, such as lymph nodes and bones (Klusa *et al.*, 2021). In the early stage of prostate cancer, most cases are asymptomatic due to the slow-growing nature of the disease, and growth in the peripheral zone of the gland (Almabrouk and Alashkham, 2024). However, problems related to the urinary system are one of the early symptoms since they occur due to the tumour pressing on the urethra. Patients may urinate more often, particularly at night, face poor urine flow, and have the occurrence of blood in urine and semen. As the cancer cells spread beyond the prostate, the patients will face a few more symptoms, such as back pain, swelling in the lower body caused by the lymph node involvement, and erectile dysfunction (Merriel *et al.*, 2018). If the cancer affects the nerves, patients may feel weakness or numbness in the legs or arms.

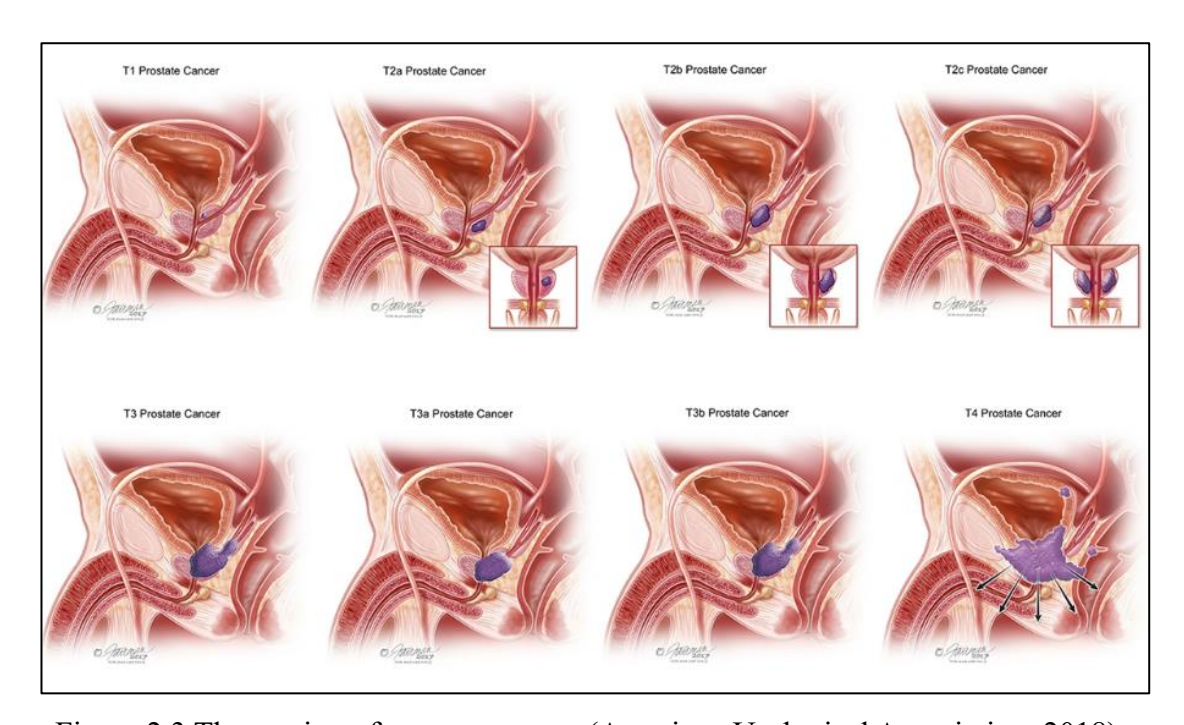


Figure 2.3 The staging of prostate cancer (American Urological Association, 2018)

Prostate cancer can be detected by doing the screening test, such as the prostate-specific antigen (PSA) test and digital rectal exam (DRE) (Abdulla and Leslie, 2024). PSA test is a common screening method, where the elevated PSA level measured in the blood indicates prostate cancer or other prostate conditions. Meanwhile, DRE is a type of physical examination that can help differentiate between benign and malignant prostate conditions (American Urological Association, 2018; Merriel *et al.*, 2018). These tests are crucial since early prostate cancer often causes no symptoms. On the other hand, the biopsy procedure, often guided by an ultrasound, is the method where the prostate tissue samples are examined under a microscope, allowing for the confirmation of the diagnosis (Rawla, 2019)

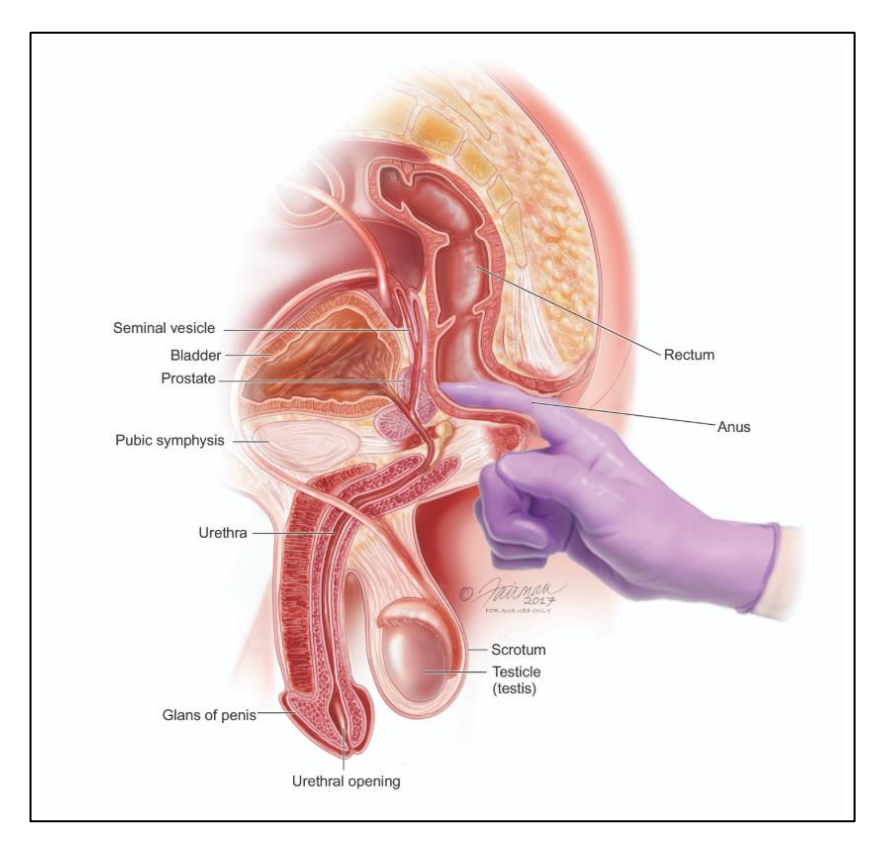


Figure 2.4 The DRE test for prostate cancer diagnosis (American Urological Association, 2018)

### 2.1.3 Treatment for Prostate Cancer

There are various options in treating prostate cancer, depending on the stage of the disease, the patient's overall health, and their preferences. When intervention is essential, the most common treatments are radical prostatectomy, or surgery. This procedure aims to prevent the illness from spreading by removing the entire prostate gland and occasionally surrounding tissues, and often when the cancer cells are within the prostate gland. The surgery can be done through open, robotic, and laparoscopic prostatectomy (Petri and McMillen, 2024).

Apart from that, radiation therapy (RT) is also one of the standard treatments to treat prostate cancer. With the aim of destroying and shrinking the cancer cells by using radiation, it can be used as the primary treatment for localised prostate cancer or in combination with other therapies (Chandra *et al.*, 2021). Particularly when surgery may not be the best option due to the patient's health or tumour location. RT can be delivered in two ways: external beam radiation therapy (EBRT) and internal beam radiation therapy (IBRT). Last but not least, hormone therapy for prostate cancer. This treatment can inhibit the growth progression of the prostate tumours by blocking the androgen activity or lowering its level. This treatment is also known as castrate-sensitive prostate cancer (National Cancer Institute, 2024)

### 2.2 Radiation Therapy

RT is a pivotal treatment technique for prostate cancer, providing both curative and palliative benefits. It uses a variety of modern approaches to target cancer cells while minimizing the impact on the surrounding healthy tissues (American Urological

Association, 2018). The advancement of RT has resulted in better patient outcomes and fewer side effects, making it a keystone in prostate cancer care.

Using a linear accelerator, EBRT, one of the RT methods, delivers high-energy X-rays or particles at the prostate from outside the body. This includes techniques like 3D conformal radiation therapy (3D CRT), intensity-modulated radiation treatment (IMRT), volumetric modulated arc therapy (VMAT), and stereotactic body radiation therapy (SBRT), which allow for accurate tumour targeting while protecting healthy tissues (Ghosh *et al.*, 2024) Furthermore, brachytherapy, where radioactive seeds are implanted directly into the prostate, is suitable for low-risk patients. It involves two types: low-dose-rate and high-dose-rate brachytherapy, distinguished by how it is delivered, the energy of the radioactive source, and the treatment period.

### 2.2.1 External Beam Radiation Therapy

To destroy the cancer cells and shrink the tumour, the EBRT is used, which involves delivering high-energy radiation supplied by a LINAC, located outside the body, to the target tumours (National Cancer Institute, 2024). EBRT provides a local treatment, meaning it targets precisely only the area of the body where the cancer is present, while sparing as much surrounding healthy tissue as possible (Cleveland Clinic, 2022; Steele *et al.*, 2021). EBRT uses a variety of energy sources, including photons, protons, electrons, and neutrons, each customised to a specific clinical circumstance (Gross *et al.*, 2015). Furthermore, modern EBRT includes conformal and intensity modulated approaches, which improve dose delivery precision and reduce exposure to important organs (Fischer-Valuck *et al.*, 2018; Le Grange, 2021).

### 2.2.2 Linear Accelerator

A linear accelerator (LINAC) is a medical device significantly used in RT to deliver high-energy X-rays or electron beams to cancer cells while minimizing exposure to healthy tissues. It is the most used machine for external beam radiation treatment beam radiation treatment can treat malignancies in almost any body area (American Association of Physicist in Medicine, 2019). LINAC uses radiofrequency (RF) electromagnetic fields to accelerate charged particles along a linear trajectory, creating more efficient techniques than the conventional electrostatic techniques in high-energy applications (Seeman *et al.*, 2020). Then, charged particles are released from a source and propelled through a sequence of cavities, where high-frequency alternating fields are applied to produce pulses of particles (Koschmieder *et al.*, 2018)

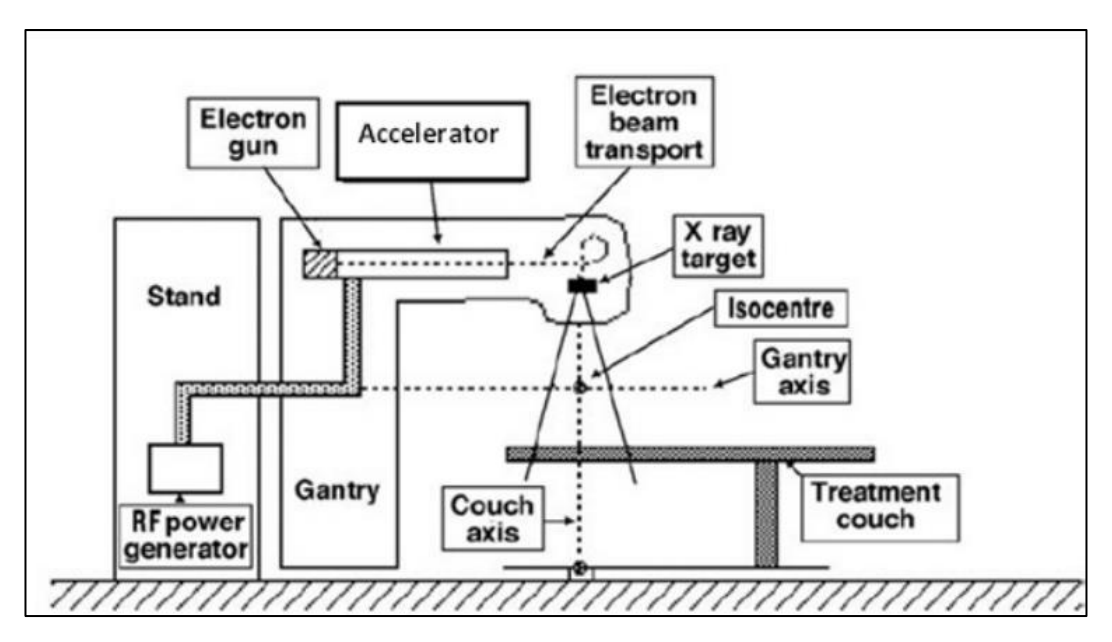


Figure 2.5 Schematic diagram of LINAC (Morrow et al., 2019)

In LINAC, electrons are generated through an electron gun, producing a stream of electrons by thermionic emission from a heated cathode. Then, these electrons are injected into a waveguide, a copper structure, and accelerated to near-light speed. This acceleration is accomplished by microwaves generated by a magnetron or klystron.

These microwaves generate oscillating electric fields within the waveguide, pushing electrons forward in synchronised bursts. As the electrons go through the waveguide, they gather kinetic energy, often reaching energies ranging from 6 to 20 megaelectron volts (MeV), depending on the therapeutic needs (Morrow *et al.*, 2019).

### 2.2.3 IMRT Treatment Technique

Advanced radiation techniques are modern approaches that have altered cancer treatment by improving accuracy and patient outcomes. One of the techniques used is IMRT, which allows for exact three-dimensional (3D) dose distribution. This action improves the precision of treatment delivered to the complex tumour (Yao and Chuan, 2024). IMRT is a type of technique that uses an inverse planning process where it starts by defining tumor and normal tissue boundaries, followed by computer optimization to create multiple small radiation fields (Mizowaki, 2015).

In highlighting the advantages of this technique, it employs multiple radiation beams to deliver a higher dose to the tumour while reducing exposure to surrounding organs, leading to improved toxicity profiles and minimizing the late effects associated with the conventional technique (Fischer-Valuck *et al.*, 2018; Le Grange, 2021). In research by Sze et al. in 2019, they highlight that IMRT can adapt to a variety of tumour sizes and patient conditions, maintaining a consistent treatment effectiveness throughout the therapy cycle (Sze et al., 2019). However, while IMRT represents a substantial improvement in radiotherapy, difficulties such as possible dosage verification mistakes and the requirement for comprehensive quality assurance remain significant issues in its use.

### 2.3 Hip Prosthesis in Radiotherapy

Some of the prostate cancer patients are found to have a hip prosthesis implant, an artificial joint that is surgically inserted and designed to fulfill the same functions as the natural one (Merola and Affatato, 2019). When arthritis, trauma, or other degenerative disorders impair the natural joint surfaces, the surgeons replace the joint with an artificial one, which is commonly made of titanium (density of 4.51 g/cm³). Since the metal density is high, it affects the X-ray attenuation and leads to inaccuracies in image reconstruction. Based on the study by Yoo et al. in 2022, artefacts can mask the significant pelvic structures, including the bladder wall, rectal shelf, and pelvic lymph nodes, potentially hiding tumours or metastases (Yoo et al., 2022). This is due to metal implants absorbing more low-energy X-rays rather than high-energy beams, causing the remaining beam to become 'hardening'. As a result, the dark and bright streaks in the reconstructed images and distortions of anatomical details mask the tumour and OAR structures (Neroladaki et al., 2019).

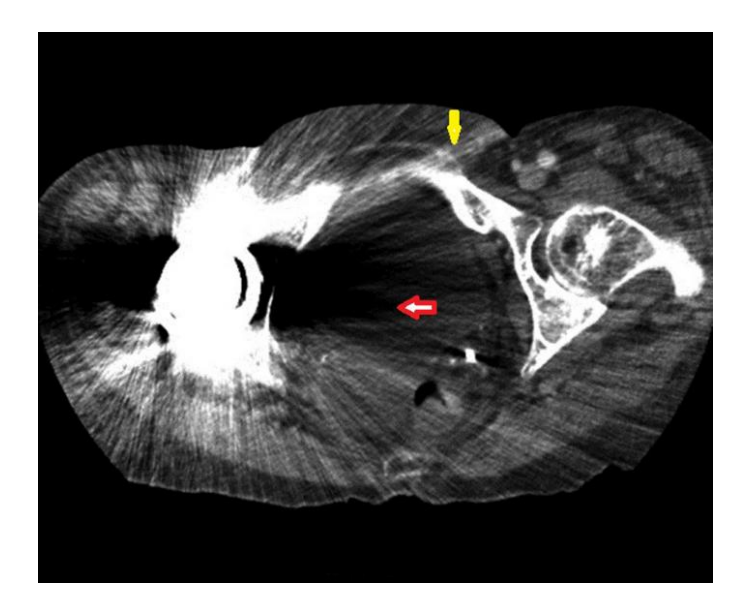


Figure 2.6 Dark streak (red arrow) and bright streak (yellow arrow) caused by a metal artefact in the CT image (Puvanasunthararajah *et al.*, 2021)

The metal artefacts in the CT images can significantly affect the dose calculation accuracy in the radiotherapy planning. The degradation of image quality caused by the streaking and distortion due to beam hardening leads to inaccurate HU and ED values in the CT image. These two parameters are essential for accurate dose calculation in RT. A study has shown that the dose errors at the isocenter can occur up to 8.4% using the artefact-affected images, which is clinically significant. For high atomic number metals, dose discrepancies in the planning target volume (PTV) can reach up to approximately 23% without artefact correction (Puvanasunthararajah *et al.*, 2021).

### 2.3.1 Metal Artifact Reduction Technique

MAR is an approach used in RT to improve the CT image quality. These techniques are intended to reduce the streaks and distortions induced by the metallic implants, such as hip prosthesis, which can degrade the dose calculation accuracy and treatment planning. Several methods have been developed, varying from conventional methods to advanced deep learning techniques, with each having its advantages and drawbacks.

Conventional methods involve modification of acquisition parameters, projection-based MAR algorithms, and using a dual-energy CT (DECT). As highlighted in research by Selles et al., in 2024, DECT uses various energy levels to distinguish between metal and surrounding tissues, enhancing image quality. The virtual monochromatic images at higher energies reduce the beam hardening effects and thus decrease the metal artefacts. This method improves the visualization of anatomy near metal implants, helping in more accurate delineation of targets and

OARs (Selles *et al.*, 2024). Another common strategy is projection-based MAR, where metal-corrupted projection data (sinograms) are identified and replaced with interpolated values from neighbouring, untouched projections. This approach is very good at reducing artefacts generated by photon starvation. Fortunately, it can sometimes generate additional, secondary streaks elsewhere in the image (Katsura *et al.*, 2018).

### 2.3.2 OMAR Algorithm in Radiotherapy

The Philips' OMAR algorithm, one of the approaches designed to mitigate the effects of metal-induced artefacts in CT images. This algorithm reduces metal artefacts by algorithmically replacing corrupted CT projections with interpolated tissue data, restoring accurate HU values and electron density. A previous study shows that OMAR reduces noise, which is the standard deviation (SD) of HU, at the region near metal implants by 30-60% compared to uncorrected images. For example, in pelvic CT scans, the SD reduced from 49.21 HU to 28.04 HU, restoring the HU values closer to the reference tissue densities (Jeong *et al.*, 2015; Puvanasunthararajah *et al.*, 2021). Besides, OMAR can reduce the dosimetric errors, and this is proven when the OMAR-corrected images decrease the dose calculation errors at the isocenter from 8.4% (uncorrected) to 2.7%-4.1% (corrected). This is crucial for avoiding under- or overdosing the targets and organs at risk (Puvanasunthararajah *et al.*, 2021).

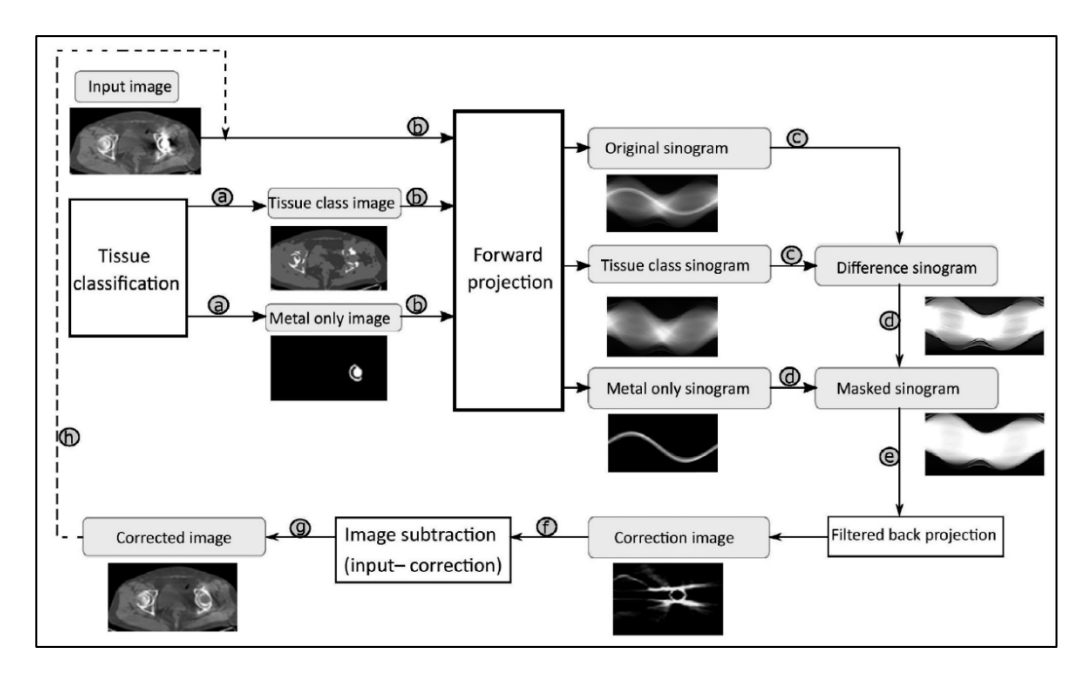


Figure 2.7 The principle of Philips' OMAR algorithm in mitigating the metal-induced artefacts in CT images (Puvanasunthararajah *et al.*, 2021)

It works through an iterative correction process that combines image segmentation and sinogram processing to minimize artefacts while preserving the actual tissue details. The algorithm starts by dividing the CT image into two components, which are a tissue class and a metal-only image. The tissue-class image shows soft tissues with uniform CT numbers, helping to reduce the variation in non-metal areas. Whereas, the metal-only image isolates pixels identified as metal, while all other pixels are set to zero.

Then, each of these images, the original, tissue class, and metal-only, is forward-projected into the sinogram domain, which represents the projection data used in CT reconstruction. A difference sinogram is calculated by subtracting the tissue-class sinogram from the original, highlighting regions affected by metal artefacts. This difference sinogram is then masked using the metal-only sinogram to isolate artefacts caused specifically by metal. The resulting masked sinogram is reconstructed using the filtered back projection to create a correction image representing the artefact component. This image is subtracted from the original CT image to produce an

artefact-reduced image. The corrected image is then used as a new input for further iterations, improving artefact suppression with each cycle (Puvanasunthararajah *et al.*, 2021).

### 2.4 Thermoluminescence Dosimeter

A thermoluminescent dosimeter (TLD) is a device that measures ionising radiation exposure by trapping energy from the radiation within its crystal lattice. When heated, the crystal releases the contained energy as visible light, within the intensity corresponding to the quantity of radiation absorbed. A specialised detector measures this light to quantify the radiation dosage to which the dosimeter was exposed. They use crystals such as lithium fluoride (LiF), or calcium sulfate doped with impurities, such as manganese, magnesium, or dysprosium, to form the trap states for electrons. Moreover, TLDs are commonly used for personal radiation monitoring, patient dose measurement, and environmental dosimetry. As shown in Figure 7, those are various forms of TLDs available, which are micro-cubes, disks, powder, threadlike, and chips.

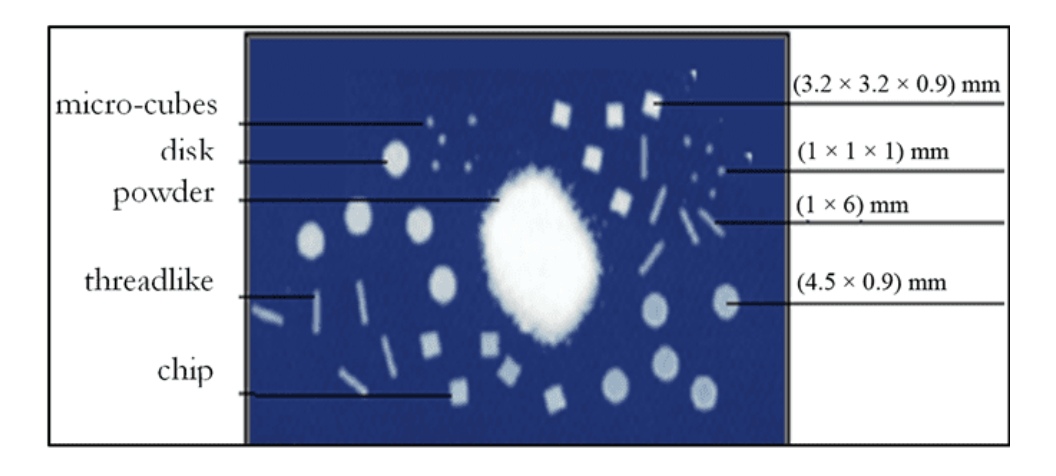


Figure 2.8 Various forms of the TLD that are commercially used

In RT, TLD is widely used to measure and verify the actual radiation doses delivered to the patients during the treatment delivery. It can be located on or within the patient's body to verify that the planned dose corresponds to the delivered dose, ensuring treatment accuracy and patient safety. Furthermore, it can be used in the tissue-equivalent phantoms to measure the point dose during the commissioning of RT machines and verification of complex treatment plans such as IMRT. The advantages of their small sizes and tissue equivalency make them ideal for dose measurement precision (Begum *et al.*, 2023).

### 2.4.1 TLD Principle

A TLD works on the basis that certain crystalline materials may trap electrons when subjected to ionising radiation. When a crystal is irradiated, the energy from the radiation excites electrons in the crystal lattice, trapping them at impurities in the crystal structure. The trapped electrons stay stable until the crystal is heated. When heated, the crystal lattice vibrates, releasing the trapped electrons, which return to their original ground state. This transition converts the stored energy into visible light, also known as thermoluminescence. The intensity of the emitted light is related to the quantity of radiation the crystal absorbs. The amount of light released during heating follows the radiation dose absorbed (Fartode *et al.*, 2019).

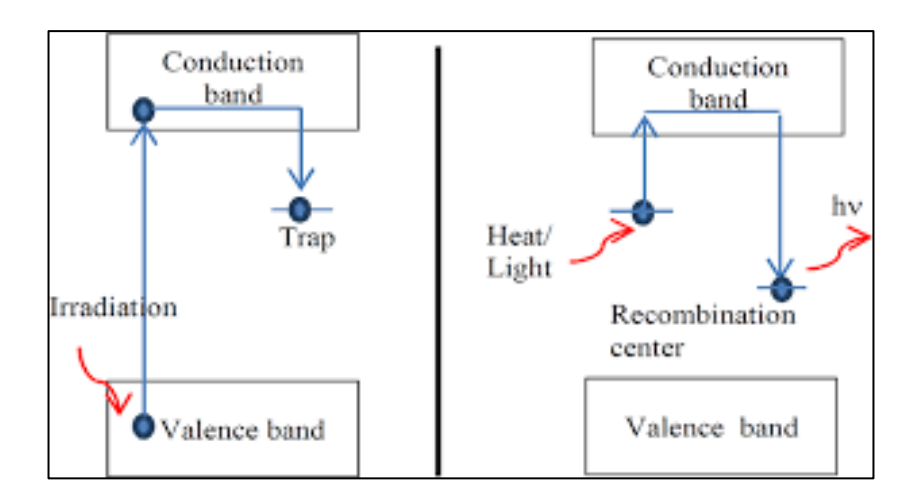


Figure 2.9 The principle of TLD

### **CHAPTER 3**

### MATERIALS AND METHODOLOGY

### 3.1 Materials

This section will give an in-depth overview of the materials employed in this study, which include physical instruments and software tools. Each item has its own significance, and they are presented in a chronological order following the approach used in this study.

### 3.1.1 TLD-100

To measure the absorbed dose of the ionising radiation, the TLD-100 dosimeter was used due to its tissue-equivalent properties, sensitivity over a broad dose range, and established reliability in clinical and research settings. The materials of the TLD-100 are composed of lithium fluoride (LiF) doped with magnesium and titanium (LiF: Mg, Ti). The TLD-100 used are in the form of chips with a size of 3.0 x 3.0 x 1.0 mm<sup>3</sup>, allowing for precise placement in the phantoms, and measuring the dose at the specific locations. The effective atomic number of this dosimeter is in the range of 5.77-6.51, which makes its radiation absorption characteristic similar to the soft tissue (7.22). This ensures that the TLD-100 provides dose measurements that are comparable to what biological tissue would absorb. The dosimeters were calibrated under the standard protocols, and their linearity and repeatability were confirmed within the experimental dose range.

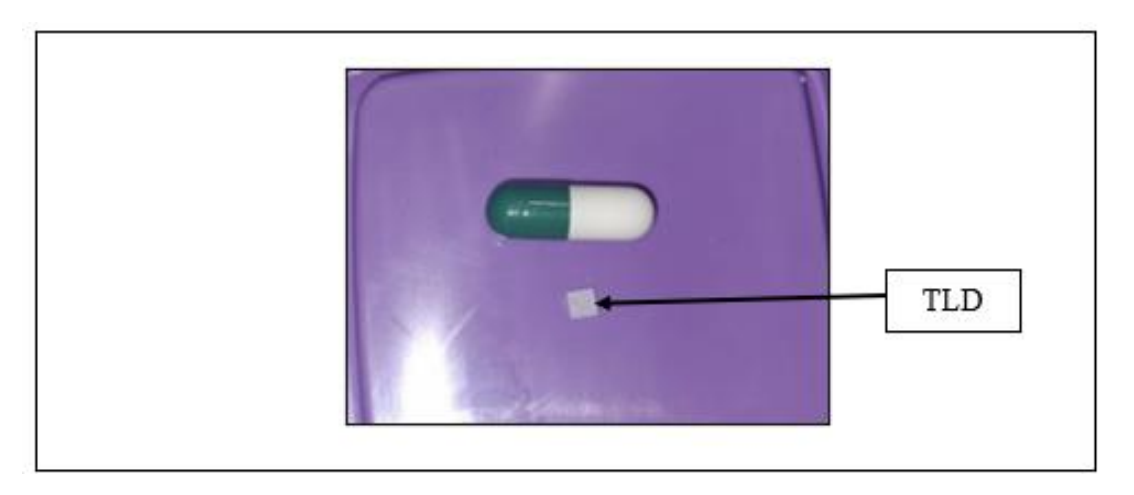


Figure 3.1 A TLD-100 chip

### 3.1.2 TLD Programmable Annealing Oven

The TLD programmable annealing oven installed at the Medical Radiation Laboratory, School of Health Science (PPSK), Universiti Sains Malaysia (USM), is model PTW T1321/U100 (PTW Freiburg, Germany). This machine is specifically designed to anneal TLDs, where the purpose is to heat the dosimeter materials to a specified temperature for a controlled period, to remove any residual radiation and prepare them for reuse. It has multiple slots that can hold three annealing trays at a time, suitable for processing large batches of TLDs.



Figure 3.2 The TLD programmable annealing oven at the Medical Radiation Laboratory, PPSK

### 3.1.3 TLD Slack and Annealing Tray

During the calibration and measurement process, the TLD slack was used to hold and carry the TLD chips. It allows the TLDs to be securely positioned and protects them during the handling, irradiation, annealing, and reading. The slack used has a dimension of 30 cm x 30 cm x 1 cm with 100 slots to hold the TLD. The TLD slack has four screws at each corner, to ensure the TLDs are securely placed within the slack.

Meanwhile, in order to anneal the TLDs, the annealing tray was used to hold and position the TLD chips within the annealing furnace during the annealing process. It is composed of steel and has 70 recesses to hold the TLDs securely during the heating. Annealing tray ensures that the TLDs are uniformly positioned and spaced for consistent and simultaneous annealing. Besides, it serves to maintain uniform

temperature exposure throughout all TLDs, resulting in residual stored energy before reuse.

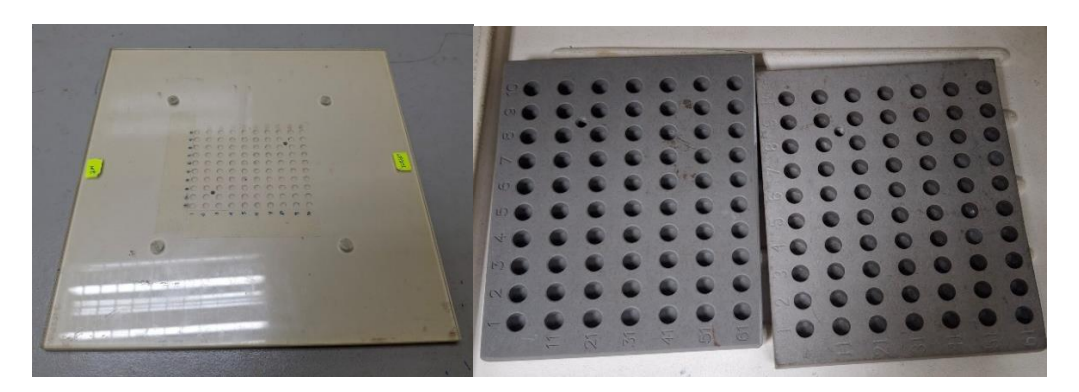


Figure 3.3 TLD slack and TLD annealing tray

### 3.1.4 TLD Reader System

The Harshaw TLD model 3500 manual reader (Thermo Fisher Scientific, Waltham, Massachusetts, United States) is installed in the Medical Radiation Laboratory, PPSK, USM, with the main role to measure and record the amount of ionising radiation exposure accumulated by the TLD chips. The features of this model TLD manual reader include a sample drawer for a single-element TLD, a linear, programmable heating system, and a cooled photomultiplier tube with corresponding electronics for measuring the TLD light output. This reader can read out various types of TLDs, such as chips, disks, rods, powders, and cubes, in a broad variety of sizes. The operational software, Thermo Scientific WinREMS, operates on a separate computer installed in the Medical Radiation Laboratory and contains the user interface, reader control, and application software.